Biogeosciences Discuss., 7, 7795–7819, 2010
www.biogeosciences-discuss.net/7/7795/2010/
doi:10.5194/bgd-7-7795-2010

Biogeosciences Discussions

MODIS observed phytoplankton dynamics in the Taiwan Strait: an absorption-based analysis

S. Shang[1], Q. Dong[2], Z. Lee[2], Y. Li[1], Y. Xie[1], and M. Behrenfeld[3]

[1]State Key Laboratory of Marine Environmental Science, Xiamen University, Xiamen 361005, Fujian, China
[2]Geosystems Research Institute, Mississippi State University, MS 39529, USA
[3]Department of Botany and Plant Pathology, Oregon State University, OR 97333, USA

Received: 25 September 2010 – Accepted: 14 October 2010 – Published: 27 October 2010

Correspondence to: S. Shang (slshang@gmail.com)

Published by Copernicus Publications on behalf of the European Geosciences Union.

Abstract

This study uses MODIS observed phytoplankton absorption coefficient (a_{ph}) as a preferable index of pigmentation to characterize phytoplankton variability in optically complex waters. We chose a quasi-analytical bio-optical inversion algorithm (QAA) to derive a_{ph} from remote sensing reflectance (R_{rs}, both in situ and MODIS measured) and then evaluated the R_{rs} derived a_{ph} by comparing them with match-up in situ measured a_{ph} collected in both oceanic and very nearshore waters in the Taiwan Strait (TWS). For the data with matching spatial and temporal window, it is found that the average percentage error (ε) between MODIS R_{rs} derived a_{ph} at 443 nm ($a_{ph}(443)$, abbreviated as *Aph*) and field measured *Aph* is 33.8% (N=30, *Aph* ranges from 0.012–0.537 m^{-1}), with a root mean square error in log scale (RMSE) of 0.226. By comparison, ε is 28.0% (N=88, RMSE=0.150) between ship-borne R_{rs} derived *Aph* and field measured *Aph*. Values of ε as large as 135.6% (N=30, RMSE=0.383) are found between MODIS R_{rs} derived chlorophyll-*a* (chl-*a*, OC3M algorithm) and field measured chl-*a*. Based on these evaluation results, we applied QAA to MODIS R_{rs} data between 2003–2009 to derive climatological monthly mean *Aph* for the TWS. Three distinct features of phytoplankton dynamics are identified. First, *Aph* is low and the least variable in the Penghu Channel, where the South China Sea water enters the TWS. This region maintains slightly higher values in winter (~17% higher than that in the other seasons) due to surface nutrient entrainment under winter wind-driven vertical mixing. Second, *Aph* is high and the most variable in the mainland nearshore water, with values peaking in summer (June–August) when river plumes and coastal upwelling enhance surface nutrient loads. Interannual variation of bloom intensity in Hanjiang River estuary in June is highly correlated with alongshore wind stress anomalies, as observed by QuikSCAT. The year of minimum and maximum bloom intensity is in the midst of an El Nino and a La Nina event, respectively. Third, a high *Aph* patch appears between April and September in the middle of the Southern TWS, corresponding to high thermal frontal probabilities, as observed by MODIS. Our results support the use of

BGD
7, 7795–7819, 2010

satellite observed *Aph* for time series analyses of phytoplankton dynamics in coastal ocean regions, where satellite chl-*a* retrievals can suffer from artifacts associated with non-biotic optically active materials.

1 Introduction

While the concentration of phytoplankton pigments in the surface ocean reflect both variability in phytoplankton standing stocks and physiological state (e.g., Behrenfeld et al., 2005; Westberry et al., 2008), it has a clear impact on the optical properties of the water, allowing its relatively straight-forward retrieval from remote sensing measurements. The most common pigment product retrieved empirically from remote sensing is chlorophyll-*a* concentration (chl-*a*), but accurate retrieval of chl-*a* can be problematic in optically complex near shore waters (Carder et al., 1989; Zhang et al., 2006). An alternative analytically retrieved property is the absorption coefficient of phytoplankton (a_{ph}), which provides a measure of photon harvesting capacity of the phytoplankton assemblage. If a_{ph} can be derived from ocean color data with less uncertainty than chl-*a*, it may function as the preferable index of pigmentation for characterizing variability in upper ocean phytoplankton, especially in optically complex waters. To test this hypothesis, we conducted a regional scale study on satellite a_{ph}, focusing on the Taiwan Strait (TWS, the area enclosed in the grey lines of Fig. 1), a shallow shelf channel that connects the South China Sea with the East China Sea (see Fig. 1).

The TWS has complex hydrographic conditions determined by the relative influence of the warm, saline, and oligotrophic South China Sea Warm Current (SCSWC) and the Kuroshio Branch Water (KBW), and the cold, fresh, and eutrophic Zhe-Min Coastal Water (ZMCW), which varies seasonally in response to changes in the monsoonal wind (e.g., Jan et al., 2002). Several medium-sized rivers (e.g., Hanjiang and Jiulongjiang Rivers) are located on the western coast (mainland China) of the strait. Also along this coast, upwelling develops in summer, driven by the prevailing southwest monsoon which runs parallel to the coast due to Ekman transport (e.g., Hong et al.,

BGD
7, 7795–7819, 2010

2009). Different waters converge in a limited area with a shallow bank (Taiwan Bank) and a ridge (Zhangyun Ridge), and a deep channel (Penghu Channel), creating strong frontal phenomena (e.g., Chang et al., 2006; Li et al., 2006).

For this study, we first derived a_{ph} from remote sensing reflectance (R_{rs}) by using a quasi-analytical bio-optical inversion algorithm (QAA, Lee et al., 2002; 2009). We then evaluated the R_{rs} derived a_{ph} data by comparing it with match-up in situ measured a_{ph} collected in both oceanic and very nearshore waters in the TWS. Finally we applied QAA to MODIS R_{rs} data for the period 2003–2009 to derive climatological monthly mean a_{ph} and to evaluate spatio-temporal variation of a_{ph} in the TWS.

2 Data

2.1 Satellite data

Aqua-MODIS daily Level-2 normalized water leaving radiance data (nLw, 2005 reprocessed version) were obtained from the NASA Distributed Active Archive Center (http://oceancolor.gsfc.nasa.gov/) and were subsequently converted to remote-sensing reflectance (R_{rs}) via the ratio of nLw to extra-terrestrial solar irradiance (F_0) (Gordon, 2005; also see http://oceancolor.gsfc.nasa.gov/DOCS/RSR_tables.html). Aqua-MODIS Level-2 chl-*a* daily data during 2003–2009 were also obtained from the same source. These data were further processed into Level-3 regional products using SeaDAS. The resolution of these data is 1 km by 1 km.

Aqua-MODIS sea surface temperature (SST) monthly mean data (4 km by 4 km resolution) during 2003–2009 were downloaded from http://oceandata.sci.gsfc.nasa.gov/. Daily wind field data were from QuikScatterometer (QuikSCAT) observations from 2003 to 2009 (http://podaac.jpl.nasa.gov), with a spatial resolution of 0.25° by 0.25° (equivalent to ~25 km by ~25 km). These data were used for calculating daily wind stress (Yelland and Taylor, 1996; Yelland et al., 1998) and monthly mean wind stress vectors for each year. Wind stress vectors were further decomposed into alongshore and cross-shore components.

BGD
7, 7795–7819, 2010

2.2 In situ data

2.2.1 Remote sensing reflectance

Spectral remote sensing reflectances (R_{rs}) were measured by using an above-water GER 1500 spectroradiometer (Spectra Vista Corporation, USA). Three measurements were made to derive R_{rs}: (1) upwelling radiance (L_u), (2) downwelling sky radiance (L_{sky}), and (3) upwelling radiance from a standard Spectralon reflectance plaque (L_{plaque}). From these three components, R_{rs} was then calculated as:

$$R_{rs} = \rho(L_u - FL_{sky})/(\pi L_{plaque}) - \Delta \quad (1)$$

where ρ is the reflectance of the Spectralon plaque (50%) and F is surface Fresnel reflectance (around 0.023 for the viewing geometry). Δ accounts for the residual surface contribution (glint, etc.), which was determined either by assuming $R_{rs}(750)=0$ (clear oceanic waters) or through iterative derivation according to optical models for coastal turbid waters as described by Lee et al. (2007).

2.2.2 Field-measured absorption coefficients and chlorophyll-*a*

Samples for determination of absorption coefficients and chl-*a* were collected from surface waters during 2003–2007 in the TWS. Sampling station depths ranged from ~10 m to ~400 m. Measurements of chromophoric dissolved organic matter (CDOM) absorption and chl-*a* were performed according to the Ocean Optics Protocols Version 2.0 (Mitchell et al., 2000), and are detailed in Hong et al. (2005) and Du et al. (2010). Particulate absorption was measured with a dual-beam PE Lambda 950 spectrophotometer equipped with an integrating sphere (150 mm in diameter) following a modified Transmittance–Reflectance (T–R) method (Tassan and Ferrari, 2002; Dong et al., 2008). This approach was used instead of the T method recommended in the NASA protocol (Mitchell et al., 2000) because some of the samples were collected near shore. Phytoplankton absorption coefficients (a_{ph}) were obtained using methanol extraction

BGD
7, 7795–7819, 2010

(Kishino, 1985). For all the field studies combined, we collected 104 sets of in situ data, with each set including total absorption (a_{t-w}, not including pure water), a_{ph}, detrital absorption (a_d), CDOM absorption (a_g) and chl-*a* (Fig. 1). This in situ dataset covers a wide range of absorption properties (Fig. 2), with $a_{t-w}(443)$ ranging from 0.019 to 2.41 m^{-1}, and the $a_{ph}(443)/a_{t-w}(443)$ ratio varying between 9–86%.

Due to frequent cloud cover in the TWS, only 30 matching data pairs were achieved of in situ absorption and chl-*a* data collected within ±24 h of MODIS overpass (Fig. 1, circle symbols). By comparison, there were 88 groups of in situ absorption and chl-*a* data having match-up in situ R_{rs} measurements (Fig. 1, cross symbols).

3 Evaluation of R_{rs} derived absorption coefficients in the Taiwan Strait

There are a series of algorithms available for the retrieval of absorption and backscattering coefficients from R_{rs}; for example, GSM (Maritorena, et al., 2002), QAA (Lee et al., 2002), and Carder_MODIS (Carder et al., 1999). Here we chose QAA_v5 to derive absorption coefficients from R_{rs} (Lee et al., 2009). Field measured R_{rs} and MODIS R_{rs} were input into the algorithm model separately to derive two sets of a_{t-w} and a_{ph}.

In order to evaluate the quality of R_{rs} derived a_{ph}, we used the root mean square in log scale (RMSE), averaged percentage error (ε), and bias as measures to describe the similarity/difference between the in situ (M) and retrieved data sets (S):

$$\varepsilon = \left(\frac{1}{n} \sum_{i=1}^{n} \left| \frac{(S)_i - (M)_i}{(M)_i} \right| \right) \times 100\% \quad (2)$$

$$\mathrm{RMSE} = \sqrt{\frac{1}{n} \sum_{i=1}^{n} (\log((S)_i) - \log((M)_i))^2} \quad (3)$$

$$\mathrm{bias} = \frac{1}{n} \sum_{i=1}^{n} [\log((S)_i) - \log((M)_i)] \quad (4)$$

BGD
7, 7795–7819, 2010

RMSE, ε, and bias results are given in Table 1. Figure 3a,b compares the derived and known a_{t-w} and a_{ph} values at 443 nm for the MODIS and the in situ data sets, respectively.

Averaged percentage error (ε) and RMSE between in situ measured $a_{ph}(412)$ and MODIS $a_{ph}(412)$ are 36.1% and 0.252, respectively, for an $a_{ph}(412)$ range of 0.009–0.539 m^{-1}. Similarly, ε is 33.8% and RMSE is 0.226 for an $a_{ph}(443)$ range of 0.012–0.537 m^{-1} (Table 1). These errors decrease when a_{ph} is derived from ship-borne R_{rs}. For example, the ε is 28.0% and the RMSE is 0.150 for 443 nm (Table 1). Such a difference is not surprising since additional uncertainties are introduced in satellite match-ups that are associated with imperfections in atmospheric correction over coastal water for the MODIS R_{rs} (Dong, 2010) and the spatio-temporal mismatch between satellite and field data (1 km^2 versus 1 m^2, and the temporal window of ±24 h) . Nevertheless, these results are even better than the global evaluation results reported in the IOCCG Report No. 5 (IOCCG, 2006), which used the earliest version of QAA (Lee et al, 2002). In that report, no satellite R_{rs} derived a_{ph} were evaluated and the RMSE between in situ R_{rs} derived $a_{ph}(443)$ and field measured $a_{ph}(443)$ was 0.321. A recent evaluation of SeaWiFS R_{rs} derived $a_{ph}(443)$ using QAA (Lee et al., 2002) at a European coastal site produced a RMSE of 0.21 (Melin et al., 2007), which is comparable to our results.

The difference between in situ measured chl-*a* and match-up R_{rs} derived chl-*a* (via OC3M) is much larger than found for $a_{ph}(443)$ (Fig. 3c). Between in situ measured chl-*a* and MODIS R_{rs} derived chl-*a*, the ε is 135.6% and RMSE is 0.383. Between in situ measured chl-*a* and in situ R_{rs} derived chl-*a*, the ε is 162.0% and RMSE is 0.429. Note that chl-*a* derived from in situ R_{rs} was calculated by using the OC3M band ratio algorithm (O'Reilly et al., 2000), consistent with that used by NASA to derive MODIS chl-*a*. Based on this analysis of match-up uncertainties, the current study indicates improved performance of MODIS-retrieved $a_{ph}(443)$ over chl-*a* with respect to assessing phytoplankton surface pigment dynamics in the TWS.

BGD
7, 7795–7819, 2010

Monthly mean $a_{ph}(443)$ (hereafter abbreviated as *Aph*) in each year and climatological monthly mean *Aph* during 2003–2009 were derived from MODIS R_{rs}, along with $a_{t-w}(443)$ from QAA-v5 and chl-*a* from OC3M (O'Reilly et al., 2000). Based on this dataset and following our previous study (Shang et al., 2005), we calculated spatial mean of *Aph*, $a_{t-w}(443)$ and chl-*a* for the TWS, where the TWS was defined as the ocean area between the China mainland coast or the 116.5° E longitude and the west coast of Taiwan, and between 22° N and 25.5° N (Fig. 1) (the same area applied to the calculation of spatial mean of QuikSCAT wind stress; see Sect. 4). We then calculated spatial anomalies (deviation from the spatial mean) of the MODIS climatological monthly mean *Aph*, $a_{t-w}(443)$ and chl-*a* for the TWS and normalized each to their respective spatial mean. The RMSD (root mean square deviation) between each pair of normalized spatial anomalies were calculated as:

$$\mathrm{RMSD} = \sqrt{\frac{1}{n}\sum_{i=1}^{n}\delta^2} \quad (5)$$

Where δ is the difference between each pair of normalized spatial anomalies, and n is the pixel number (varies from 134 000 to 148 118, depending on percentage of cloud cover in each month). As shown in Fig. 4, the RMSD is larger between *Aph* and chl-*a* than between $a_{t-w}(443)$ and chl-*a*, especially during the cold season when the wind is strong and the water is relatively turbid due to sediment resuspension (Guo et al., 1991). This finding clearly indicates that the spatial pattern of empirically derived chl-*a* is more similar to that of $a_{t-w}(443)$ than *Aph*. Thus, the empirical chl-*a* product is registering the combined influence of phytoplankton pigments and other optically active materials (detritus and CDOM) in the TWS, similar as that found in the South Pacific Gyre (Lee et al., 2010). This finding again suggests the use of MODIS *Aph* data as the preferable phytoplankton pigment index in the optically complex coastal water of the TWS.

BGD
7, 7795–7819, 2010

4 Spatio-temporal variation of MODIS *Aph* in the Taiwan Strait

Climatological monthly mean *Aph* data reveals significant spatio-temporal variations of *Aph* during 2003–2009 (Fig. 5). The standard deviation of annual mean *Aph* identifies a highly variable area located alongshore the China mainland, and an area showing low temporal variation located in the deepest zone of the TWS (i.e. the Penghu Channel), adjacent to the South China Sea (Fig. 6a).

To investigate further the seasonality of *Aph* in waters of low temporal variation, we chose a square in the Penghu Channel (right bottom of Fig. 6a) and derived its monthly time series. Although variations are weak, we do find that *Aph* slightly increases during December to March by about 17% over the mean level of *Aph* in the other months (Fig. 6b). This seasonal pattern with a winter maximum is similar to in situ observations of chl-*a*, phytoplankton cell counts, and primary production at SEATS (18° N 116° E, South East Asian Time-series Study station, Tseng et al., 2005) and the entire South China Sea (Ning et al., 2004; Chen, 2005). This correspondence between seasonal cycles of phytoplankton pigment in the TWS and South China Sea is not surprising since this part of the TWS is dominated by the SCSWC (Jan et al., 2002). Enhanced nitrate availability in winter due to enhanced wind driving vertical mixing is thought to play a role in modulating phytoplankton dynamics in this water (Chen, 2005), although photoacclimation and altered grazing pressure may also be important (Behrenfeld et al., 2005; Behrenfeld, 2010).

In contrast to the Penghu Channel water, *Aph* is highly variable alongshore the China mainland, influenced by inputs of the Jiulongjiang and Hanjiang Rivers (see locations in Fig. 1) and by upwelling in summer (Hong et al., 2009) and the Zhe-Min Coastal Water in winter (Jan et al., 2002). In the nearshore band west of the white line on Fig. 6a, *Aph* ranges from 0.048 m^{-1} in March to 0.088 m^{-1} in June (Fig. 6b). Overall, *Aph* peaks in summer (June–August) at a value 64% higher than the minimum *Aph* observed in spring (March–May). Summer is the season of peak river flow, which accounts for 44% of the annual discharge (Sun et al., 2009; http://baike.baidu.com/

BGD
7, 7795–7819, 2010

view/23372.html). Summer is also the season of southwesterly wind, which drives coastal upwelling (Hong et al., 2009). Nearshore phytoplankton blooms, as indexed by the high *Aph* values, are thus supported by the availability of nutrients provided by both river plumes and upwelling.

A close-up view of this nearshore water in May–August (Fig. 7a) clearly demonstrates the combined impacts of river plume and upwelling in summer. Out of each estuary, there is a tongue of high *Aph* (generally $\geq 0.1\,m^{-1}$) advecting northeastward. This feature is most distinct in June (Fig. 7a). In the vicinity of Hanjiang River estuary (also nearby the Dongshan Island), a broad area of especially high *Aph* is found, relative to values for the Jiulongjiang River estuary. This difference is, in part, due to the volume of Hanjiang River annual flow at $258\times10^9\,m^3$, which is ~80% higher than the Jiulongjiang River ($142\times10^9\,m^3$) (Sun et al., 2009). In addition, a significant upwelling center is located in the vicinity of Dongshan Island (Hong et al., 2009). These combined factors (upwelling and stronger river plume) result in stronger blooms for the Hanjiang River estuary area.

To investigate the bloom intensity variation for such an upwelling enhanced bloom in the Hanjiang River estuary area, an annual areal bloom index (ABI) was used. ABI was calculated as the sum of *Aph* at pixels having $Aph \geq 0.1\,m^{-1}$ for all valid observations in a month (*Aph* of $0.1\,m^{-1}$ corresponds to $\sim 1.7\,mg\,m^{-3}$ chl-*a* in the TWS (Dong, 2010)). The ABI within a square representing the Hanjiang River estuary (see location on the June image of Fig. 7a; its area is $9400\,km^2$) in June of each year during 2003–2009 is shown in Fig. 7b. The ABI peaks in 2008 and is the lowest in 2004, and is well correlated with the alongshore wind stress anomaly (deviations from the area-averaged climatological monthly means). More positive alongshore wind stress anomalies correspond to stronger southwesterly winds, which drive enhanced upwelling, offshore advection of river plumes, and stronger phytoplankton blooms (and vise versa). However, the ABI in 2009 is $152\,m^{-1}$, even lower than the ABI in 2003 ($776\,m^{-1}$). The alongshore wind stress anomaly is positive in 2009 and negative in 2003, suggesting bloom favoring conditions in 2009 compared to 2003. This abnormally low number in

BGD
7, 7795–7819, 2010

2009 is in part due to missing satellite data in the Hanjiang River estuary area owing to heavy cloud cover. Totally, there are 7771 pixels in the square for ABI estimation. During most of the year, more than 80% of the pixels in the square have valid retrievals; while in 2009, only 29% of the pixels have valid *Aph* data (Fig. 7b). Therefore, additional uncertainties of satellite data due to bad weather conditions must be noted, necessitating careful examination of the data.

Interestingly, the year of the lowest ABI (2004) is in the midst of an El Nino event (2000–2005), and the year of the highest ABI (2008) is in the midst of a La Nina event (2007–2009), as indicated by the Multivariate ENSO Index (MEI, http://www.cdc.noaa.gov/people/klaus.wolter/MEI/; Fig. 7b). Such an ABI difference between El Nino and La Nina years might be more significant, if it is influenced by potential differences in cloud cover between El Nino and La Nina years, since 78% of the total pixels have valid retrievals in 2008 while the percentage of valid retrievals is as high as 86% in 2004 (Fig. 7b). It has been acknowledged that the relationship between the Asian monsoon and ENSO is mutual but selectively interactive (e.g., Webster and Yang 1992); however, which is the cause and which is the effect remain unclear (e.g., Kinter III, et al., 2002). Here we observed a strong coastal bloom in 2008, when the southwest monsoon was the strongest (during 2003–2009) and a La Nina event was occurring. We also observed a weak bloom in 2004, when the southwest monsoon was the weakest (during 2003–2009) and an El Nino event was at its mid-point. Further study of regional scale ecosystem variability should advance understanding of the monsoon-ENSO interaction.

Spatial anomalies of *Aph* highlight a very distinct high *Aph* patch generally located in the middle of the Southern TWS, appearing in the period of April to September (Fig. 8a). This patch is most probably associated with (1) shelf break upwelling in the vicinity of the Taiwan Bank (Li et al., 2000), (2) island stirring around Penghu Islands (Simpson and Tett, 1986) and (3) upwelling associated with Zhangyun Ridge (Pi and Hu, 2010). Frontal probabilities derived from MODIS SST during 2003–2009, which were calculated by applying the approach of Wang et al. (2001), are grater than 60%

BGD
7, 7795–7819, 2010

in the area corresponding to this *Aph* patch (Fig. 8b). Since vertical temperature gradients are smaller during cold seasons, these fronts can only be well developed in the surface water during warm seasons (April–September). Fronts provide powerful physical forcings to inject nutrients from deep water into the surface, thus facilitating phytoplankton growth.

5 Conclusions

The current study provides both an assessment of algorithm performance and a description of phytoplankton dynamics in the optically complex TWS. Based on our analysis of 104 in situ measurements in the TWS, we find that the QAA algorithm provides a satisfactory assessment of a_{ph} from both MODIS and ship borne R_{rs}. Then we derive climatological monthly mean *Aph* (2003–2009) from MODIS R_{rs} with QAA and find a variety of seasonal patterns for *Aph* in the TWS. The most interesting result is that the phytoplankton bloom in the vicinity of Hanjiang River estuary, which is enhanced by upwelling in summer, shows an order of magnitude variation between years (2003–2009). This interannual variability is highly correlated with alongshore wind stress anomalies and ENSO activities, and demonstrates ecological responses to changing in environmental forcings, documented here for the first time, through employment of satellite *Aph* data. It should be noted, however, that some uncertainties remain in our satellite a_{ph} products due to issues with variable cloud cover that may introduce biases in our results, especially in winter. Repeated observations from multi-sensors and geostationary satellites may help resolve such problems in the future.

Acknowledgements. This work was supported jointly by the High-tech R&D program of China (#2008AA09Z108), NSF-China (#40976068), the National Basic Research Program of China (#2009CB421200 and 2009CB421201), the China Scholarship Council, and the Program of ITDU (#B07034). We thank the crew of the R/V Yanping II, and J. Wu, X. Ma, X. Sui, W. Zhou, W. Wang, M. Yang, C. Du and G. Wei for their help in collecting in situ data and Drs. Allen Milligan and Toby Westberry for helpful discussions during our analysis.

BGD
7, 7795–7819, 2010

References

Behrenfeld, M. J., Boss, E., Siegel, D. A., and Shea, D. M.: Carbon-based ocean productivity and phytoplankton physiology from space, Global Biogeochem. Cy., 19, GB1006, doi:10.1029/2004GB002299, 2005.

Behrenfeld, M. J.: Abandoning Sverdrup's Critical Depth Hypothesis on phytoplankton blooms, Ecology, 91, 977–989, 2010.

Carder, K. L., Steward, R. G., Harvey, G. R., and Ortner, P. B.: Marine humic and fulvic acids: their effects on remote sensing of ocean chlorophyll, Limnol. Oceanogr., 34, 68–81, 1989.

Carder, K. L., Chen, F. R., Lee, Z., Hawes, S. K., and Kamykowski, D.: Semianalytic Moderate-Resolution Imaging Spectrometer algorithms for chlorophyll-*a* and absorption with bio-optical domains based on nitrate-depletion temperatures, J. Geophys. Res., 104, 5403–5421, 1999.

Chang, Y., Shimada, T., Lee, M. A., Lu, H. J., Sakaida, F., and Kawamura, H.: Winter-time sea surface temperature fronts in the Taiwan Strait, Geophys. Res. Lett., 33, L23603, doi:10.1029/2006GL027415, 2006.

Chen, L.: Spatial and seasonal variations of nitrate-based new production and primary production in the South China Sea, Deep-Sea. Res. Pt. I, 52, 319–340, 2005.

Dong, Q., Hong, H., and Shang, S.: A new approach to correct for pathlength amplification in measurements of particulate spectral absorption by the quantitative filter technique, J. Xiamen Univ. (Nat. Sci.), 47, 556–561, 2008 (in Chinese, with English abstract).

Dong, Q.: Derivation of phytoplankton absorption properties from ocean color and its application, Ph.D., Xiamen University (China), 2010.

Du, C., Shang, S., Dong, Q., Hu, C., and Wu, J.: Characteristics of Chromophoric Dissolved Organic Matter in the nearshore waters of the Western Taiwan Strait, Estuar. Coast. Shelf. S., 88, 350–356, 2010.

Gordon, H. R.: Normalized water-leaving radiance: revisiting the influence of surface roughness, Appl. Opt., 44, 241–248, 2005.

Guo, L., Hong, H., Chen, J., and Hong, L.: Distribution and variation of suspended matter in the Southern Taiwan Strait, in: Minnan-Taiwan Bank Fishing Ground Upwelling Ecosystem Study, edited by: Hong, H., Science Press, Beijing, China, 273–281, 1991 (in Chinese, with English abstract).

Hong, H., Wu, J., Shang, S., and Hu, C.: Absorption and fluorescence of chromophoric dissolved organic matter in the Pearl River Estuary, South China, Mar. Chem., 97, 78–89, 2005.

BGD
7, 7795–7819, 2010

Hong, H., Zhang, C., Shang, S., Huang, B., Li, Y., Li, X., and Zhang, S.: Interannual variability of summer coastal upwelling in the Taiwan Strait, Cont. Shelf. Res., 29 , 479–484, 2009.
Jan, S., Wang, J., Chern, C. S., and Chao, S. Y.: Seasonal variation of the circulation in the Taiwan Strait, J. Marine Syst., 35, 249–268, 2002.
Kinter III, J., Miyakoda, K., and Yang, S.: Recent change in the connection from the Asian monsoon to ENSO, J. Climate, 15, 1203–1215, 2002.
Kishino, M., Takahashi, M., Okami, N., and Ichimura, S.: Estimation of the spectral absorption coefficients of phytoplankton in the sea, B. Mar. Sci., 37, 634–642, 1985.
Lee, Z., Carder, K. L., and Arnone, R. A.: Deriving inherent optical properties from water color: a multiband quasi-analytical algorithm for optically deep waters, Appl. Opt., 41, 5755–5772, 2002.
Lee, Z.: Remote sensing of inherent optical properties: fundamentals, tests of algorithms, and applications, IOCCG (International Ocean-Colour Coordinating Group) Rep No. 5, Dartmouth, Canada, 2006.
Lee, Z., Carder, K. L, Arnone, R. A, and He, M.: Determination of primary spectral bands for remote sensing of aquatic environments, Sensors, 7, 3428–3441, 2007.
Lee, Z., Lubac, B., Werdell, J., and Arnone, R.: An update of the Quasi-Analytical Algorithm (QAA_v5), available at: http://www.ioccg.org/groups/Software_OCA/QAA_v5.pdf, 2009.
Lee, Z., Shang, S., Hu, C., Lewis, M., Arnone, R., Li, Y., and Lubac, B.: Time series of bio-optical properties in a subtropical gyre: implications for the evaluation of inter-annual trends of biogeochemical properties, J. Geophys. Res., 115, C09012, doi:10.1029/2009JC005865, 2010.
Li, C., Hu, J., Jan, S., Wei, Z., Fang, G. H., and Zheng, Q.: Winter-spring fronts in Taiwan Strait, J. Geophys. Res., 111, C11S13, doi:10.1039/2005JC003203, 2007.
Li, L., Guo, X., and Wu, R.: Oceanic fronts in Southern Taiwan Strait, J. Oceanogr. Taiwan Strait, 19, 147–156, 2000 (in Chinese, with English abstract).
Maritorena, S., Siegel, D. A., and Peterson, A. R.: Optimization of a semianalytical ocean color model for global-scale applications, Appl. Optics, 41, 2705–2714, 2002.
Melin, F., Zibordi, G., and Berthon, J. F.: Assessment of satellite ocean color products at a coastal site, Remote. Sens. Environ., 110, 192–215, 2007.
Mitchell, B. G., Bricaud, A., and Carder, K.: Determination of spectral absorption coefficients of particles, dissolved material and phytoplankton for discrete water samples, in: Ocean Optics Protocols for Satellite Ocean Color Sensor Validation, revision 2, edited by: Fargion, G. S.

BGD
7, 7795–7819, 2010

and Mueller, J. L., NASA Goddard Space Flight Space Center, Greenbelt, Maryland, 125–153, 2000.
Ning, X., Chai, F., Xue, H., Cai, Y., Liu, C., and Shi, J.: Physical-biological oceanographic coupling influencing phytoplankton and primary production in the South China Sea, J. Geophys. Res., 109, C10005, doi:10.1029/2004JC002365, 2004.
O'Reilly, J. E., Maritorena, S., Siegel, D., and O'Brien, M. C.: Ocean color chlorophyll-*a* algorithms for SeaWiFS, OC2, and OC4: version 4, in: SeaWiFS Postlaunch Technical Report Series, Vol. 11, SeaWiFS Postlaunch Calibration and Validation Analyses, Pt. 3, edited by: Hooker, S. B. and Firestone, E. R., NASA Goddard Space Flight Center, Greenbelt, Maryland, 9–23, 2000.
Pi, Q. and Hu, J.: Analysis of sea surface temperature fronts in the Taiwan Strait and its adjacent area using an advanced edge detection method, Sci. China Ser. D, 53, 1008–1016, 2010.
Shang, S., Zhang, C., Hong, H., Liu, Q., Wong, G. T. F., Hu, C., and Huang, B.: Hydrographic and biological changes in the Taiwan Strait during the 1997–1998 El Nino winter, Geophys. Res. Lett., 32, L11601, doi:10.1029/2005GL022578, 2005.
Simpson, J. H. and Tett, P.: Island steering effects on phytoplankton growth, in: Lecture Notes on Coastal and Estuarine Studies, edited by: Bowman, J., Yentsch, M., and Peterson, W. T., Springer-Verlag, Berlin, 41–76, 1986.
Sun, B., Zhou, G., Wei, H., Liu, Z., and Zeng, D.: The flux of river active material flowing into the sea: preliminary achievements, Earth Sci. Frontiers, 16, 361–368, 2009 (in Chinese, with English abstract).
Tassan, S. and Ferrari, G. M.: A sensitivity analysis of the "Transmittance-Reflectance" method for measuring light absorption by aquatic particles, J. Plankton. Res., 24, 757–774, 2002.
Tseng, C. M., Wong, G. T. F., Lin, I. I., Wu, C. R., and Liu, K. K.: A unique seasonal pattern in phytoplankton biomass in low-latitude waters in the South China Sea, Geophys. Res. Lett., 32, L08608, doi:10.1029/2004GL022111, 2005.
Wang, D. X., Liu, Y., Qi, Y. Q., and Shi, P.: Seasonal variability of thermal fronts in the Northern South China Sea from satellite data, Geophys. Res. Lett., 28, 3963–3966, 2001.
Webster, P. and Yang, S.: Monsoon and ENSO: selectively interactive systems, Q. J. Roy. Meteor. Soc., 118, 877–926, 1992.
Westberry, T., Behrenfeld, M. J., Siegel, D. A., and Boss, E.: Carbon-based primary productivity modeling with vertically resolved photoacclimation, Global. Biogeochem. Cy., 22, GB2024, doi:10.1029/2007GB003078, 2008.

BGD
7, 7795–7819, 2010

Yelland, M. J. and Taylor, P. K.: Wind stress measurements from the open ocean, J. Phys. Oceanogr., 26, 541–558, 1996.

Yelland, M. J., Moat, B. I., Taylor, P. K., Pascal, R. W., Hutchings, J., and Cornell, V. C.: Wind stress measurements from the open ocean corrected for airflow distortion by the ship, J. Phys. Oceanogr., 28, 1511–1526, 1998.

Zhang, C., Hu, C., Shang, S., Muller-Karger, F. E., Li, Y., Dai, M., Huang, B., Ning, X., and Hong, H.: Bridging between SeaWiFS and MODIS for continuity of chlorophyll-*a* concentration assessments off Southeastern China, Remote. Sens. Environ., 102, 250–263, 2006.

BGD

7, 7795–7819, 2010

Table 1. Error statistics between derived and *in situ* absorption coefficients and 437 chlorophyll-*a* data*.

Band (nm)		RMSE	bias	ε (%)	R^2	n
Derived from in situ measured R_{rs} (N=88)						
a_{t-w} (λ)	412	0.155	−0.052	26.1	0.80	88
	443	0.135	−0.046	23.1	0.87	88
	488	0.117	−0.013	22.4	0.93	88
	531	0.169	0.061	37.7	0.91	88
a_{ph} (λ)	412	0.145	0.004	26.9	0.86	88
	443	0.150	0.014	28.0	0.87	88
	488	0.189	0.088	43.0	0.90	88
	531	0.348	0.258	116.1	0.85	88
chl-*a*		0.429	0.268	162.0	0.80	88
Derived from MODIS R_{rs} (N=30)						
a_{t-w} (λ)	412	0.150	−0.037	25.9	0.76	30
	443	0.127	−0.068	21.1	0.91	30
	488	0.109	−0.018	20.2	0.91	30
	531	0.142	−0.002	25.7	0.91	30
a_{ph} (λ)	412	0.252	−0.168	36.1	0.87	25
	443	0.226	−0.147	33.8	0.86	25
	488	0.265	−0.059	34.8	0.87	28
	531	0.267	0.070	63.5	0.88	26
chl-*a*		0.383	0.237	135.6	0.81	30

* N is the number of data tested, while n is the number of valid retrievals.

BGD
7, 7795–7819, 2010

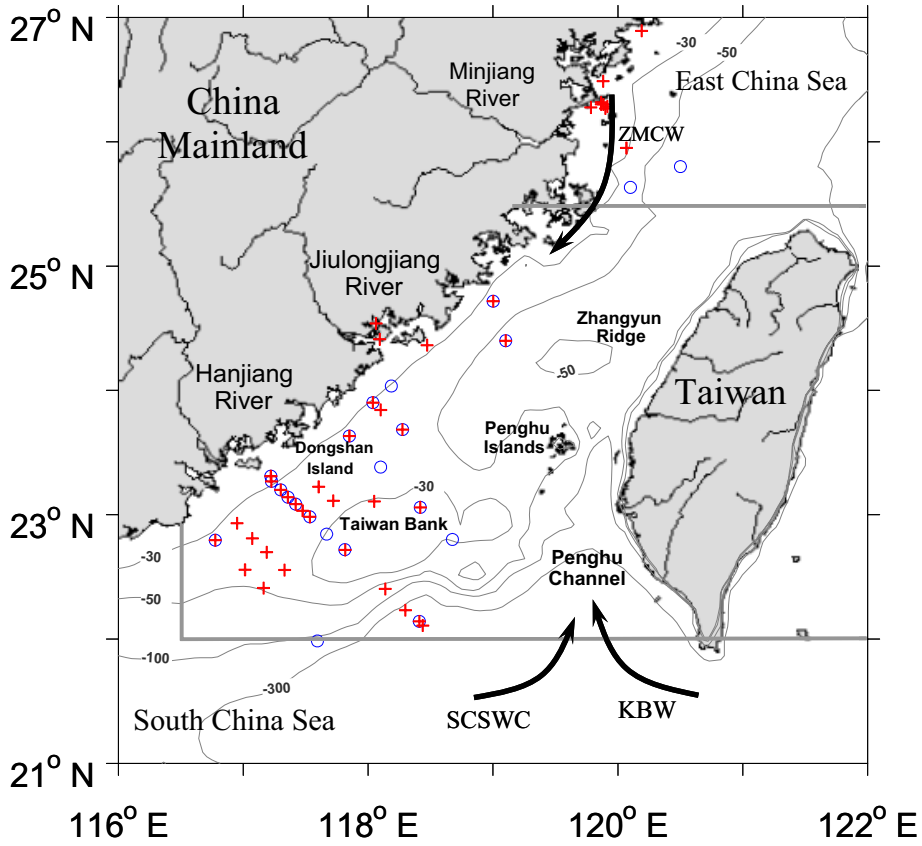

Fig. 1. Map of the Taiwan Strait; ZMCW: Zhe-Min Coastal Water; SCSWC: South China Sea Warm Current; KBW: Kuroshio Branch Water; the cross and circle symbols show the locations where in situ measured R_{rs} and MODIS R_{rs} have match-up in situ observed absorption coefficients, respectively; the grey lines indicate the 446 boundaries of the research area of this study.

BGD
7, 7795–7819, 2010

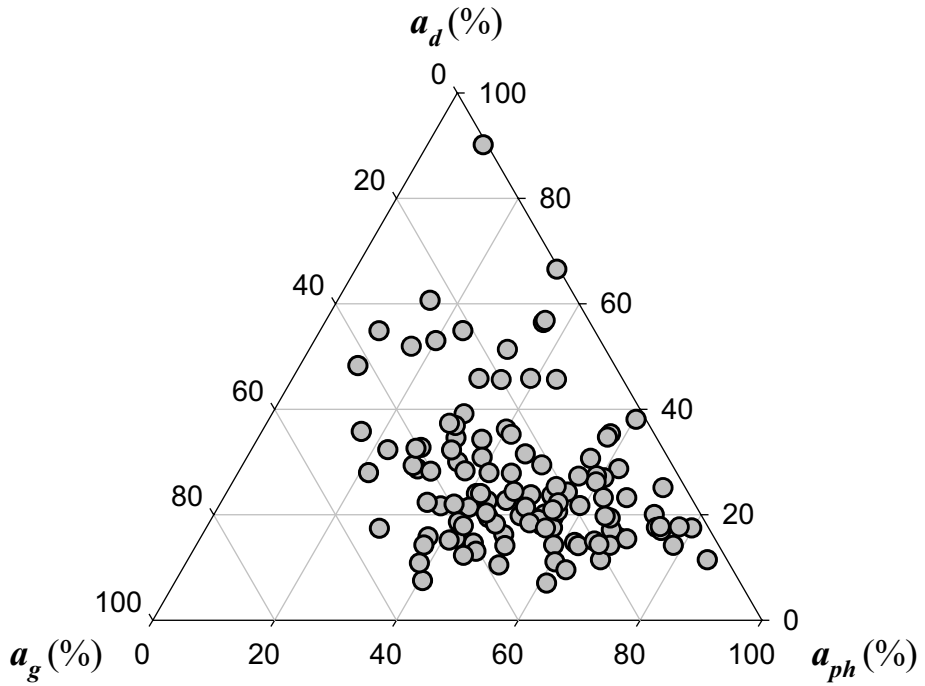

Fig. 2. The proportion of a_{ph}, a_d and a_g in total absorption at 443 nm.

BGD
7, 7795–7819, 2010

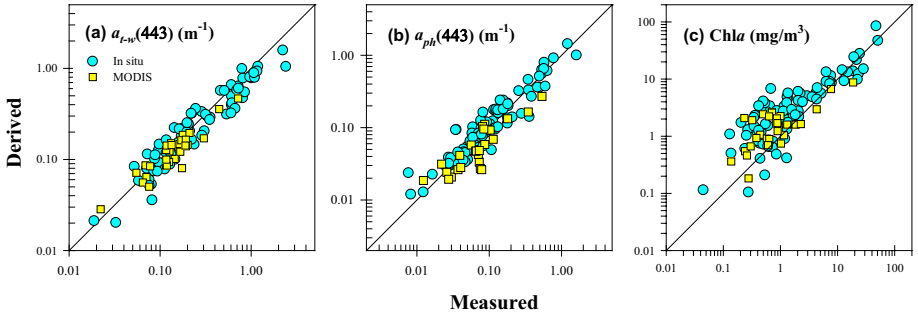

Fig. 3. Scatter plot of R_{rs} (both in situ and MODIS) derived **(a)** $a_{t-w}(443)$, **(b)** $a_{ph}(443)$ and **(c)** chl-*a* versus field measured data.

BGD
7, 7795–7819, 2010

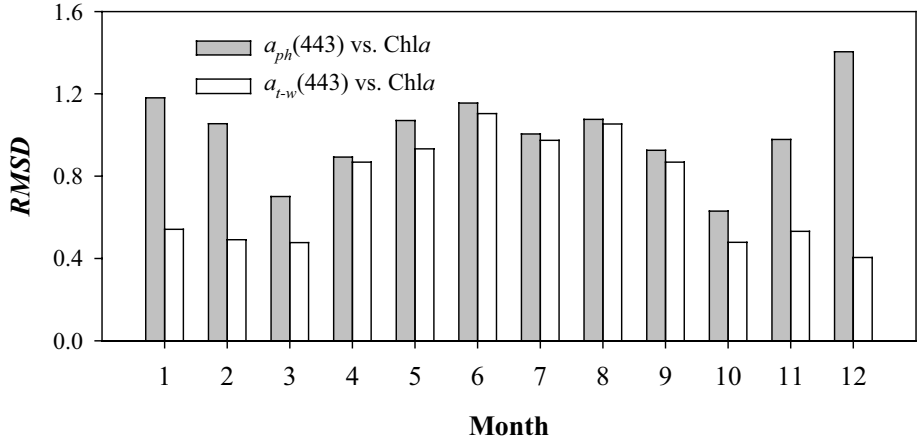

Fig. 4. Root mean square deviation between normalized spatial anomaly of $a_{ph}(443)$ and that of chl-*a*, and normalized spatial anomaly of $a_{t-w}(443)$ and that of chl-*a*.

BGD
7, 7795–7819, 2010

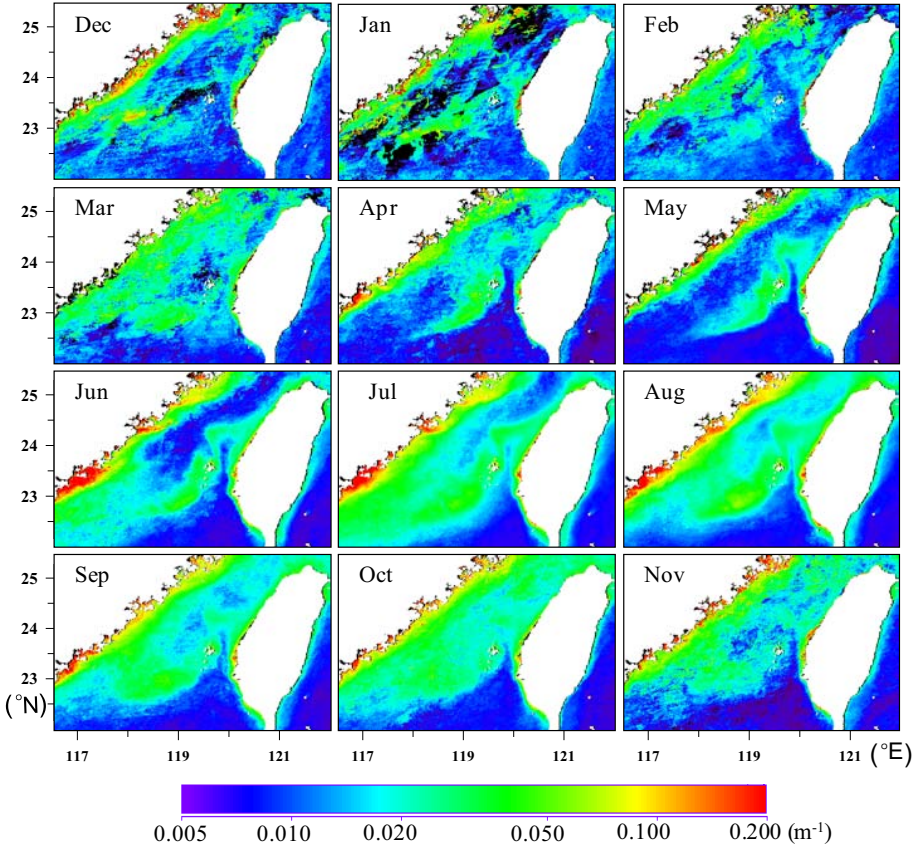

Fig. 5. Multi-year monthly mean MODIS *Aph* in the Taiwan Strait (2003–2009).

BGD
7, 7795–7819, 2010

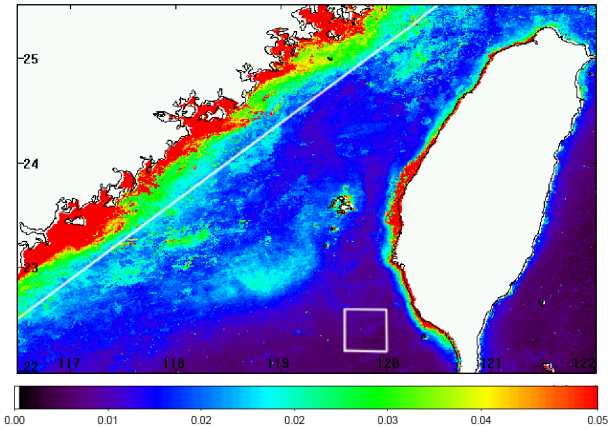

Fig. 6. **(a)** Annual mean standard deviation of *Aph*; **(b)** the annual cycle of *Aph* in the most variable (west of the white line alongshore on Fig. 6a) and least variable (the square at the right bottom of Fig. 6a) areas.

BGD
7, 7795–7819, 2010

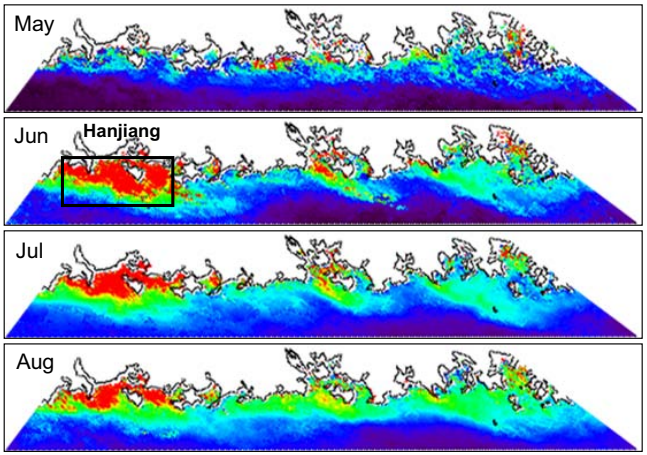

(a)

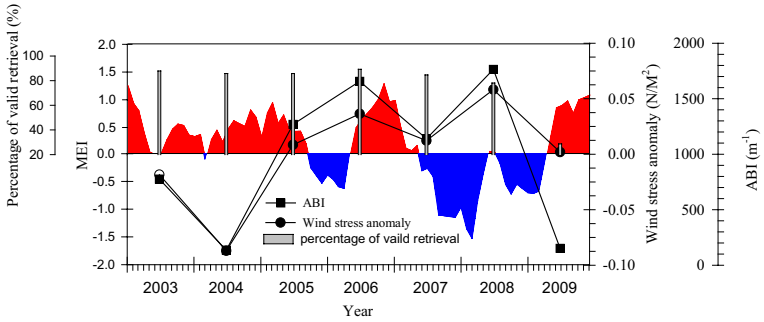

(b)

Fig. 7. (a) A close-up view of *Aph* in the nearshore water (west of the white line alongshore on Fig. 6a) in May–August; **(b)** the interannual variation of *Aph* percentage of valid retrievals and alongshore wind stress anomaly in the area of Hanjiang River estuary in June during 2003–2009 and the MEI.

BGD
7, 7795–7819, 2010

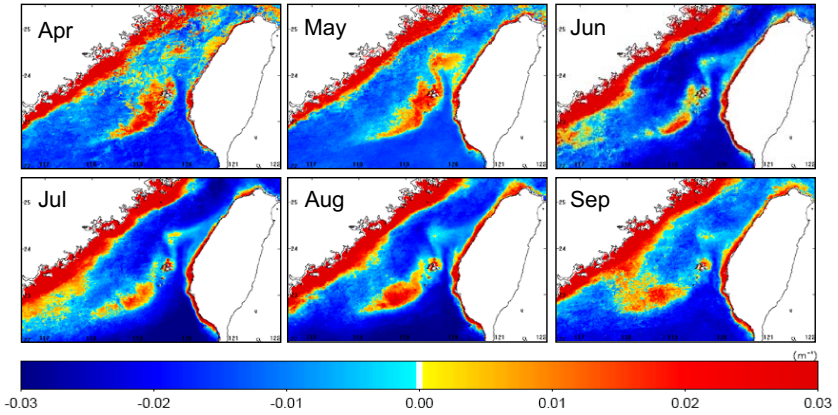

(a)

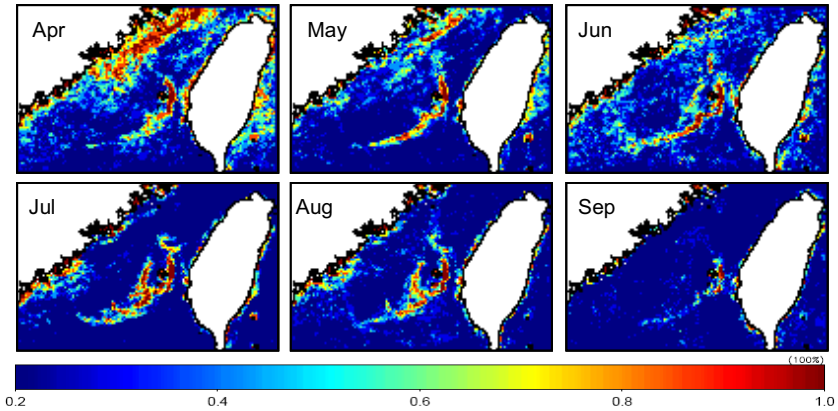

(b)

Fig. 8. (a) Spatial anomaly of *Aph* in the TWS in April–September; **(b)** thermal frontal probability in April–September.

BGD
7, 7795–7819, 2010